Guided locally optimal control of quantum dynamics in dissipative environments

Jean Christophe Tremblay* and Peter Saalfrank†
Institut für Chemie, Universität Potsdam, Karl-Liebknecht-Straße 24-25, D-14476 Potsdam-Golm, Germany
(Received 30 September 2008; published 5 December 2008)

We present ideas for controlling quantum dynamics in a dissipative environment using short, intense laser pulses. The proposed algorithm is an extension of the well-established time-local pump-dump control scheme to the density matrix formalism, using time-dependent targets. This provides a natural framework for guiding the reaction along a desired path. As a test case, the selective photoexcitation of charge transfer and semi-charge-transfer states of the LiCN molecule in a strong dissipative environment is studied.

DOI: 10.1103/PhysRevA.78.063408 PACS number(s): 32.80.Qk, 33.80.−b, 02.30.Yy

I. INTRODUCTION

In the past decades optical quantum control of chemical reactions has attracted considerable interest [1,2]. Different solutions have been proposed to study, drive, and characterize theoretically the very complex dynamics of small quantum systems. Among the numerous approaches advocated by theoreticians, the simplest one is to use analytical pulses such as π pulses. These are known to work for population control in nondissipative few-level systems and can be adapted by iterative parameter variation for more complicated systems. A great step forward is the so-called coherent control [3–6]. In this framework one uses the knowledge of the system to intuitively design analytical pulses to achieve a specific target, exploiting interference effects between competing reaction paths. The elegance of this approach has the disadvantage of making the study of large systems difficult, where the many competing reaction paths cannot easily be simultaneously taken into account.

Optimal control theory (OCT) represents a good alternative for such intricate cases [7–17]. Selective pulses are found iteratively by maximizing a global cost functional designed to achieve specific targets while respecting a certain number of constraints, such as maintaining a low optimal field fluence. Each iteration requires forward and backward propagations, and many cycles are usually necessary to converge to a mathematical solution of the design equations. Due to the numerical burden associated with such calculations, the algorithm becomes rapidly unstable as the system size increases. Furthermore, to describe open systems, one usually uses the reduced density matrix approach, as is the case for the Redfield and Lindblad theories [18], or uses a stochastic description for energy relaxation and dephasing [19–21]. The backward propagation can become unstable when dealing with nonreversible systems, as part of the energy is lost to the environment upon forward time propagation and gained during backward propagation. As a result, most of the optimal control calculations for dissipative systems to date were restricted to few-level systems.

To circumvent this problem it is possible to use local optimization procedures [8,22–28]. The main advantage comes from the fact that no backward propagation is required, which stabilizes the algorithm and renders it more efficient. The stability is recovered at the expense of finding a solution to a control equation which is valid only locally in time. These methods are well established for propagating wave packets representing isolated systems and we propose to extend these ideas to the reduced density matrix formalism.

An optimal control variant of the local time algorithm was recently published [29]. The idea is to divide the full interval into small subintervals and to optimize the cost functional on the subinterval. For that purpose, so-called moving targets, i.e., time-dependent target operators, were used to steer the reaction along a desired path. Moving targets have been previously used [30,31]. It was found that the optimal subinterval size was equal to the time step size used for integrating the equations of motion [29]. In Ref. [29] it was also observed that within a subinterval many fewer forward-backward propagations were needed than for global OCT on a single interval. As a consequence, the stability of the algorithm improves.

In the present paper we propose to use moving targets within a purely time-local optimization framework without any backward propagation. The time-dependent targets will be used as a tool for guiding the reaction along a preferred pathway, which is reminiscent of the coherent control idea. The control equation is derived as a perturbation to a rationally designed field, the "reference field" $E_{\mathrm{ref}}(t)$, which further stabilizes the algorithm. We dub our approach guided locally optimal control theory (GLOCT).

The paper is organized as follows. In the next section we derive the equations for the proposed guided local control scheme. The system of interest, the dissipation model, and the associated equations of motion will be described briefly in Sec. III. In Sec. IV we perform selective excitations of charge transfer states of an embedded LiCN molecule and analyze the algorithm's behavior. The most important results are then summarized in Sec. V.

II. GUIDED LOCALLY OPTIMAL CONTROL THEORY

In order to maximize the expectation value of a time-dependent guide operator $\hat{G}(t)$ at the end of a laser pulse of duration t_f, we choose to define the cost functional

*jean.c.tremblay@gmail.com
†petsaal@rz.uni-potsdam.de

$$J[E(t)] = \langle\langle \hat{G}(t_f)|\hat{\rho}(t_f)\rangle\rangle + \int_0^{t_f} \frac{1}{\alpha(t)}|E(t) - E_{\text{ref}}(t)|^2 dt. \quad (1)$$

Here, $E(t)$ is an electric field, $E_{\text{ref}}(t)$ a reference field to be specified below, and $\hat{\rho}(t)$ the reduced density operator representing a system of interest coupled to an environment. Further, $\alpha(t)$ is a user-specified function to weight the significance of the second term. Finally, double space notation has been used to define the dot product of two operators in the Liouville space, i.e., $\langle\langle \hat{A}|\hat{B}\rangle\rangle = \text{Tr}\{\hat{A}^\dagger \hat{B}\}$.

There are many ways of optimizing Eq. (1) locally, e.g., by using OCT with time-dependent targets or a conjugate gradient to numerically solve the design equation. The first approach requires backward propagation at each time step, whereas the second one might require a few iterations to converge. We advocate a simpler procedure, which yields an analytical expression for the locally optimal electric field. Following Ohtsuki *et al.* [25], we rewrite the equation as

$$J[E(t)] = \int_0^{t_f} \frac{d}{dt}[\langle\langle \hat{G}(t)|\hat{\rho}(t)\rangle\rangle]dt + \int_0^{t_f} \frac{1}{\alpha(t)}|E(t) - E_{\text{ref}}(t)|^2 dt + \langle\langle \hat{G}(0)|\hat{\rho}(0)\rangle\rangle. \quad (2)$$

The function $\hat{G}(t)$ is chosen as a linear operator and the derivative on the right-hand side can be expanded to yield

$$J[E(t)] = \int_0^{t_f} \left[\langle\langle \dot{\hat{G}}(t)|\hat{\rho}(t)\rangle\rangle + \langle\langle \hat{G}(t)|\dot{\hat{\rho}}(t)\rangle\rangle + \frac{1}{\alpha(t)}|E(t) - E_{\text{ref}}(t)|^2 \right] dt + \langle\langle \hat{G}(0)|\hat{\rho}(0)\rangle\rangle, \quad (3)$$

where the overdots indicate time derivatives. We know that the evolution of the system obeys the Liouville–von Neumann equation, given in the semiclassical dipole approximation by

$$\frac{\partial \hat{\rho}(t)}{\partial t} = -\frac{i}{\hbar}[\hat{H}_0, \hat{\rho}(t)] + \frac{i}{\hbar}E(t)[\hat{\mu}, \hat{\rho}(t)] + \mathcal{L}_D\hat{\rho}(t). \quad (4)$$

Here, $\hat{H}_0$ is the unperturbed Hamiltonian, $\hat{\mu}$ is the system's dipole operator, and $\mathcal{L}_D$ is the dissipative Liouvillian superoperator, which will be discussed later. Replacing the derivative of the density operator in Eq. (3) by (4), we obtain

$$J[E(t)] = \int_0^{t_f} \left(\langle\langle \dot{\hat{G}}(t)|\hat{\rho}(t)\rangle\rangle - \frac{i}{\hbar}\langle\langle \hat{G}(t)|[\hat{H}_0, \hat{\rho}(t)]\rangle\rangle + \frac{i}{\hbar}E(t)\langle\langle [\hat{\mu}, \hat{\rho}(t)]\rangle\rangle + \langle\langle \hat{G}(t)|\mathcal{L}_D\hat{\rho}(t)\rangle\rangle + \frac{1}{\alpha(t)}|E(t) - E_{\text{ref}}(t)|^2 \right) dt + \langle\langle \hat{G}(0)|\hat{\rho}(0)\rangle\rangle. \quad (5)$$

Minimizing the functional using a conventional variational procedure,

$$\frac{\delta J[E(t)]}{\delta E(t')} = \lim_{\eta\to 0} \frac{J[E(t) + \eta\delta(t - t')] - J[E(t)]}{\eta} = 0, \quad (6)$$

we obtain a simple expression for the locally optimal field as a correction to a reference field,

$$E(t) = E_{\text{ref}}(t) + \alpha(t)\langle\langle \hat{G}(t)|\hat{\mu}\ \text{Im}[\rho(t)]\rangle\rangle. \quad (7)$$

The function $\alpha(t)$ is chosen so that the field vanishes at times $t=0$ and t_f, if this condition also holds for the reference field:

$$\alpha(t) = \alpha_0 \sin^2\left(\frac{\pi t}{t_f}\right). \quad (8)$$

Here, α_0 is a user-defined parameter. In the present formulation it is very simple to further constrain the amplitude of the resulting field directly by setting, at each time step, $E(t) = \min[E(t), E_{\max}]$. In the end, the field is thus restricted in this work to a plateau shape with $\lim_{t\to 0} E(t) = \lim_{t\to t_f} E(t) = 0$ (see below). Of course, this restriction is made for "practical" reasons and can be relaxed if desired. The resulting locally optimized field can be analyzed using its Husimi transform $P_H(t, \epsilon)$ [32], which is a Gaussian smoothing of the Wigner quasi-probability distribution giving time- (t) and energy- (ϵ) resolved information. For more details, see for example Refs. [33,34].

A natural but otherwise arbitrary choice for the guiding function $\hat{G}(t)$ is the desired time-dependent population evolution of the system. Choosing to populate one or, sequentially, several of the L eigenstates of the system, we have

$$\hat{G}(t) = \sum_{k=0}^{L-1} O_{kk}(t)\hat{P}_k, \quad (9)$$

where $\hat{P}_k = |k\rangle\langle k|$ is the projector on state k. Of course, choices other than (9) are possible. The time-dependent weights $O_{kk}(t)$ are chosen here either as $O_{kk}(t)=0$ if state k is not to be populated, or as Gaussian functions centered at time t_k and with variance σ_k,

$$O_{kk}(t) = N(t)e^{-(t-t_k)^2/2\sigma_k^2}, \quad (10)$$

where $N(t)$ is a factor ensuring that the target operator is normalized at any given time. Whereas conjugate gradient procedures and OCT with moving targets optimize numerically the time-dependent cost functional to strictly mimic the desired reaction path, the present approach follows this "guide" as an analytical solution to the design equation—merely a "suggestion" for the actual reaction path. This increased flexibility in conjunction with the amplitude constraint should allow us to obtain experimentally realizable optimal fields.

III. THE DISSIPATIVE TIME-DEPENDENT CONFIGURATION INTERACTION METHOD AND ITS EQUATIONS OF MOTION

In order to test this guided locally optimal control theory, we study the selective excitation of charge transfer states of a linear lithium cyanide molecule in a strong dissipative envi-

ronment. This is performed using the time-dependent configuration interaction approach [35], as applied to the density matrix to treat open systems [36]. For that purpose we define the field-free electronic Hamiltonian $\hat{H}_0$ representing N electrons in the field of N_A nuclei. The nuclei are assumed to be fixed at their equilibrium geometry on the whole excitation time scale, which ranges up to 1 ps. The electronic eigenvalue problem $\hat{H}_0\Psi_i=E_i\Psi_i$ is solved using standard configuration interaction methodology. We first use the ground state Slater determinant Ψ_0^{HF} to compute the spatial orbitals at the restricted Hartree-Fock level. The full Hamiltonian is represented in a basis of singly excited configurations Ψ_r^a, which are generated by exciting one electron from occupied orbitals a to unoccupied orbitals r. In the present work we perform laser-induced dipole switching experiments of singlet states of LiCN, and only the corresponding excited configurations ${}^1\Psi_a^r=(1/\sqrt{2})(\Psi_a^r+\Psi_{\bar{a}}^{\bar{r}})$ ($\{a,r\}$ refer to α and $\{\bar{a},\bar{r}\}$ to β spin orbitals) were considered for the calculations. The diagonalization of the resulting Hamiltonian matrix yields the configuration interaction singles (CIS) energies E_i^{CIS} and wave functions Ψ_i, which are given by

$$\Psi_i = D_{0,i}\Psi_0^{\mathrm{HF}} + \sum_{a=L}^{N/2}\sum_{r=N/2+1}^{M} D_{a,i}^r\,{}^1\Psi_{a,r}, \tag{11}$$

where $D_{k,i}$ are expansion coefficients, L is the index of the lowest occupied orbital, and M that of the highest unoccupied orbital. The CIS energies are then further corrected by perturbative inclusion of double excitations, giving CIS(D) energies $E_i^{\mathrm{CIS(D)}}=E_i^{\mathrm{CIS}}+E_i^{(\mathrm{D})}$ where $E_i^{(\mathrm{D})}$ is defined elsewhere [36,37].

The CIS(D) eigenfunctions and energies are subsequently used to represent the density operator compactly. We choose to propagate the density matrix in the interaction representation [36], i.e., $\hat{\rho}(t)=e^{i\hat{H}_0t/\hbar}\hat{\rho}^I(t)e^{-i\hat{H}_0t/\hbar}$. In the basis of the CIS eigenstates, the equations of motion for the reduced density operator then become

$$\frac{d\rho_{mn}^I}{dt} = \frac{i}{\hbar}E(t)\sum_{j=1}^{L}(e^{-i\omega_{mj}t}\mu_{mj}\rho_{jn}^I - e^{-i\omega_{jn}t}\rho_{mj}^I\mu_{jn}) + e^{-i\omega_{mn}t}\langle m|\mathcal{L}_D\hat{\rho}|n\rangle, \tag{12}$$

where L is now the number of CIS(D) eigenstates and $\hbar\omega_{mn}=E_m^{\mathrm{CIS(D)}}-E_n^{\mathrm{CIS(D)}}$ the energy difference between states m and n. ρ_{mn}^I is the $\{m,n\}$ element of the density matrix in the interaction picture and $\mu_{mn}=\langle\Psi_m|\hat{\mu}|\Psi_n\rangle$ is the associated dipole matrix element. [The vector character of the dipole operator $\hat{\mu}$ and of the field $E(t)$ is neglected for the moment; see further below.] The equations of motion are solved numerically using a Cash-Karp Runge-Kutta integrator with adaptive step size [36,38,39]. Due to the varying time steps the problem is highly nonlinear. This is more than compensated by the self-controlled error mechanism of the embedded Runge-Kutta algorithm, which ensures internal consistency of the propagation on the whole time interval.

The energy dissipation in this so-called open system is studied using the semigroup formalism, introduced by Kossakowski and co-workers [40,41]. In particular we use here the Lindblad formalism [42], which ensures semipositivity of the reduced density matrix and thus allows interpretation of its diagonal elements as populations of the associated states. We simulate the effect of energy relaxation in an electron-rich environment such as a metal surface using raising and lowering operators [36,43], and we choose to neglect the effects of pure dephasing. In the basis of the subsystem eigenstates, the matrix elements of the appropriately defined dissipative Liouvillian are then given by [36]

$$\langle n|\mathcal{L}_D\hat{\rho}|n\rangle = \sum_{j=1}^{L}(\Gamma_{j\to n}\rho_{jj} - \Gamma_{n\to j}\rho_{nn}), \tag{13}$$

$$\langle m|\mathcal{L}_D\hat{\rho}|n\rangle = -\frac{1}{2}\sum_{j=1}^{L}(\Gamma_{m\to k}+\Gamma_{n\to k})\rho_{mn} \quad \text{if } m\neq n. \tag{14}$$

Here, $\Gamma_{m\to n}$ is the transition rate between states m and n. Rather than calculating the latter from a specific microscopic model, we simply evaluate the downward transition rates by scaling the Einstein coefficients for spontaneous emission as

$$\Gamma_{m\to n} = \frac{n|\mu_{mn}^{\mathrm{tot}}|^2}{3\pi\hbar\epsilon_0 c^3}\omega_{mn}^3. \tag{15}$$

Here, c is the speed of light, ϵ_0 its electric permittivity, and $|\mu_{mn}^{\mathrm{tot}}|=(\mu_{mn,x}^2+\mu_{mn,y}^2+\mu_{mn,z}^2)^{1/2}$ the total transition dipole moment. The factor n is the refractive index ($n=1$ in vacuum) which we interpret here as a scaling factor to mimic the presence of a dissipative medium. In the following we set $n=10^5$. This gives rise to lifetimes of a few hundreds of femtoseconds, which are not unusual for surface reactions. Upward transitions are forbidden at zero temperature, which is assumed here. For more details on the present dissipation model, the reader is referred to Ref. [36].

IV. SELECTIVE CHARGE TRANSFER AND DISSIPATIVE SUBSYSTEM DYNAMICS IN LiCN

A. The model

For controlled electron dynamics in a dissipative environment, the same model as in Ref. [36] has been used. In order to obtain the CIS(D) energies, all calculations are made by fixing the geometry of the molecule at its Hartree-Fock (HF) 6-31G* optimized equilibrium value (see Fig. 1). The system is originally prepared in the ground state, which has a permanent dipole moment of $-3.7082ea_0$, to simulate experiments at low temperature. Only singlet states are accessible from this singlet ground state. Accordingly, only those are considered in the present study. A set of 186 singlet states is obtained at energies below $5E_h$. All of these are used in the calculations below. It was demonstrated that one must include many more states than those involved in the photoinduced processes to obtain converged electron dynamics when short, intense laser pulses are used [44]. The 185 excited singlet states lie relatively close to each other and dynamic broadening due to the intensity of the laser field should thus affect the selectivity of the excitations. Further,

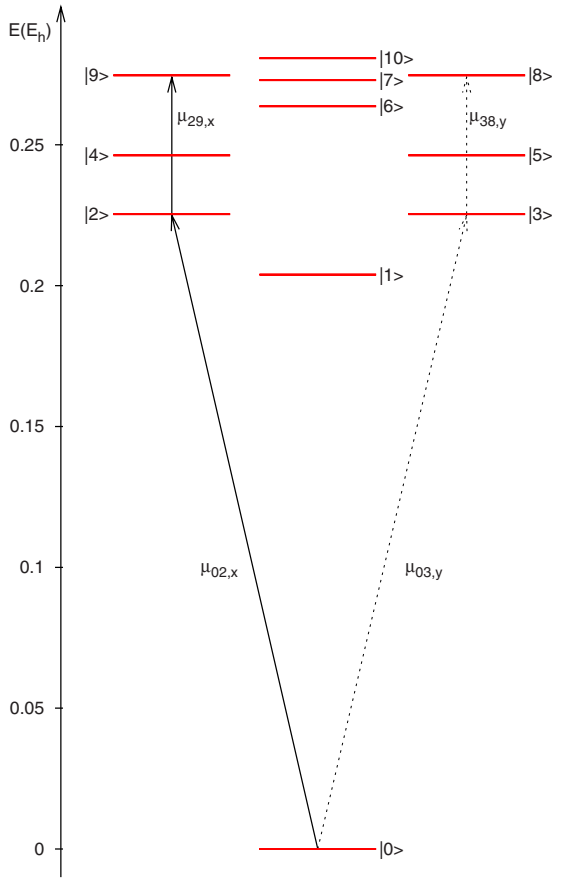

FIG. 1. (Color online) First few electronic eigenenergies of the LiCN molecule calculated at the CIS(D) 6-31G* level of theory. The eigenstates on the left (right) are accessible using x-polarized (y-polarized) fields, and those in the center using z-polarized fields.

since the control algorithm has more reaction paths and undesirable product states to take into account, the minimization procedure becomes more challenging.

We are mainly interested in exciting the first doubly degenerate transfer state, labeled $\{|2\rangle,|3\rangle\}$, which has a permanent dipole moment of $+2.7952ea_0$. Assuming that the molecule is oriented along z, the $|0\rangle \rightarrow |2\rangle$ transition is strongly x polarized, and $\mu_{02,x}=0.3084ea_0$. (The degenerate $|0\rangle \rightarrow |3\rangle$ transition is strongly y polarized.) An intramolecular charge transfer occurring during the $|0\rangle \rightarrow |2\rangle$ transition is responsible for the sign reversal of the dipole moment. The excitation energy $\hbar\omega_{02}$ is $0.2254E_h$ (6.13 eV). Using the current dissipation model, the charge transfer state $|2\rangle$ has a lifetime of $\tau_{20}=\Gamma_{2\rightarrow 0}^{-1}=430$ fs.

Subsequently we populate the doubly degenerate semicovalent transfer state, labeled $\{|8\rangle,|9\rangle\}$, which possesses a lifetime of $\tau_{92}=\Gamma_{9\rightarrow 2}^{-1}=3.6$ ps and a dipole moment of $-1.1777ea_0$ due a partial back transfer of negative charge from the Li to the CN part of the molecule. Also the $|2\rangle \rightarrow |9\rangle$ transition is dominantly x polarized with $\mu_{29,x}=-1.0333ea_0$, while the degenerate state $|8\rangle$ is almost completely y polarized. The excitation energy is $\hbar\omega_{29}=0.0493E_h$ (1.34 eV). Being interested in x-polarized transitions only, in the following we will adopt x-polarized light only such that $E(t)$ and μ_{mn} in Eq. (12) are the x components of field and transition dipole moment only. A more detailed analysis of the system can be found in Ref [37]. It is interesting to note that both states of interest possess a lifetime larger than that of the first $z-$ polarized state $|1\rangle$, $\tau_{10}=\Gamma_{1\rightarrow 0}^{-1}=260$ fs.

For all calculations the reference field is chosen as a series of x-polarized π pulses, each tailored to completely transfer the population in an ideal two-level system without dissipation:

$$E_{\mathrm{ref}}(t)=\sum_{i=1}^{n} U_i(t)\cos(\omega_i t),$$

$$U_i(t)=\begin{cases} E_{0i}\sin^2\left(\dfrac{\pi(t-t_{i_1})}{t_{i_2}-t_{i_1}}\right) & \text{if } t_{i_1}\leqslant t\leqslant t_{i_2}, \\ 0 & \text{otherwise.} \end{cases} \tag{16}$$

t_{i_1} (t_{i_2}) is the ith pulse's starting (finishing) time, ω_i the carrier frequency (chosen resonant with the respective transition), and $E_{0i}=2\pi\hbar/[(t_{i_2}-t_{i_1})\mu_i]$ the maximal field amplitude for the ith transition (μ_i is the corresponding transition dipole moment). Note that only states $|2\rangle$ and $|9\rangle$ are accessible using an x-polarized electric field and that no population is found in states $|3\rangle$ and $|8\rangle$ at the end of all our tailored pulses, as expected.

B. Population of a charge transfer state

Figure 2 shows the population evolution for the excitation of the charge transfer state $|2\rangle$. The locally optimal control field and its Husimi transform are shown in the top two panels, with $\alpha_0=0.1E_h/(ea_0)^2$ and $E_{\max}=0.001E_h/ea_0$ (5.14 MV/cm). The guide operator $\hat{G}$ was defined by Eqs. (9) and (10) with only two nonvanishing projectors, the ground state at $t_0=0$ fs and state $|2\rangle$ at $t_2=1000$ fs, both with variance $\sigma_j=300$ fs and properly normalized, $\hat{G}=O_{00}(t)|0\rangle\langle 0|+O_{22}(t)|2\rangle\langle 2|$. With this choice a smooth transition from the ground state to the charge transfer state is anticipated, to be completed after the control time $t_f=1000$ fs. The reference field E_{ref} was chosen as a single π pulse for the $0\rangle \rightarrow |2\rangle$ transition, starting at $t_1=0$ and ending at $t_2=t_f$.

It is clear from the lower panel that this is a strong dissipative environment. The 1 ps pulse is much longer than the state lifetime of 430 fs. The GLOCT pulse yields about 42.9% population transfer to the desired state, as compared to 37.3% for the simple π pulse, while the field fluence remains realistically small at 13.1 mJ/cm^2. For the π pulse, the fluence is 3.2 mJ/cm^2. It can be seen that the electric field strictly respects the maximal amplitude constraint. It is interesting to note that the pulse peak amplitude is shifted toward the end of the time interval. Whereas the reference field is composed of a single frequency centered at the $|0\rangle \rightarrow |2\rangle$ transition, the GLOCT pulse presents three components. The ω_{02} transition still dominates strongly over the whole interval, but field contributions centered at about $\frac{1}{3}\omega_{02}$, and to a lesser extent at $\sim\frac{1}{4}\omega_{02}$, can also be seen. It could be rationalized that the intensity of the laser field makes mul-

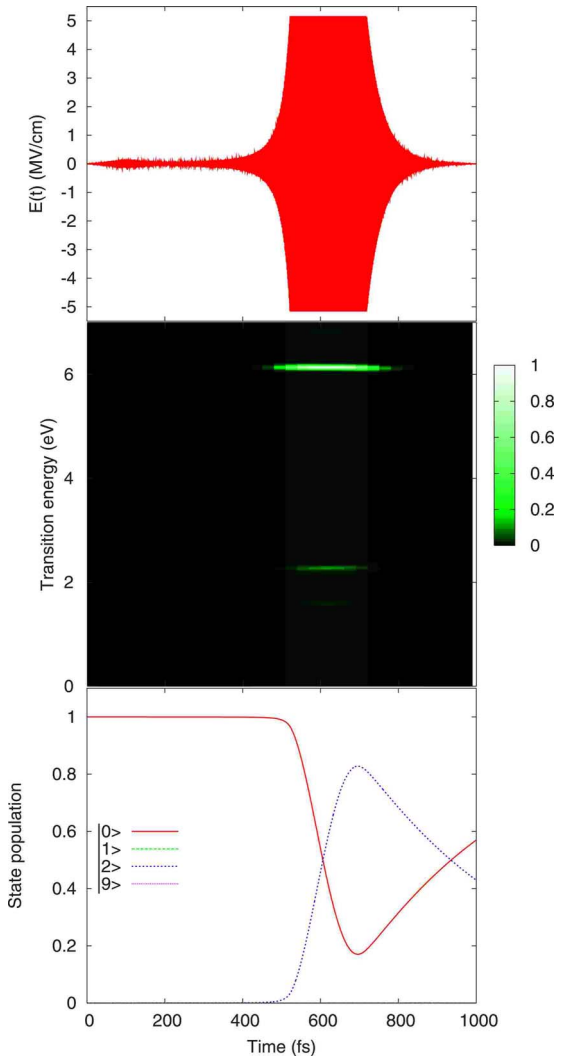

FIG. 2. (Color online) Population evolution (bottom panel), electric field (top panel), and its Husimi transform (central panel) for the excitation of state $|2\rangle$ using a 1 ps laser pulse. Local control parameters: $\alpha_0=0.1E_h/(a_0)^2$ and $E_{\max}=0.001E_h/ea_0$ (5.14 MV/cm).

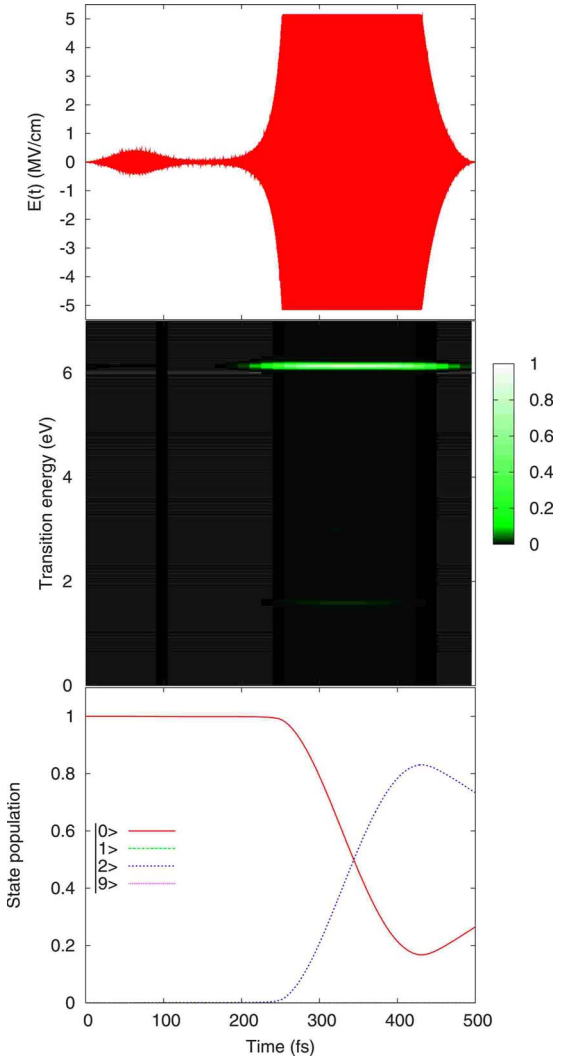

FIG. 3. (Color online) Population evolution (bottom panel), electric field (top panel), and its Husimi transform (central panel) for the excitation of state $|2\rangle$ using a 500 fs laser pulse. Local control parameters: $\alpha_0=0.1E_h/(a_0)^2$ and $E_{\max}=0.001E_h/ea_0$ (5.14 MV/cm).

tiple photon transitions possible, or that constructive interference between the different reaction paths improves the transfer rate. It remains that the relatively small number of frequency contributions in the field would make it, most probably, experimentally realizable. Note that, since the field components are far apart, it is conceivable that multiple light sources tuned at different frequencies would be necessary to achieve such a control pulse.

We tried to design a shorter pulse of 500 fs to counter the effects of dissipation and improve the transfer yield. The field restriction parameters α_0 and $E_{\max}$ were kept the same and the guide operator parameters were modified to $t_0=0$ fs, $t_2=500$ fs, and $\sigma_j=100$ fs. The reference field was a π pulse of length 500 fs and a fluence of 6.4 mJ/cm^2.

Figure 3 shows the resulting pulse and the associated population evolution. As expected, the transfer yield is greatly improved by such simple manipulation, reaching 73.4% at the end of the propagation compared to only 60.9% for a π pulse of the same duration. The field fluence (11.9 mJ/cm^2) is comparable to that of the longer pulse but the transfer yield is considerably higher. This does not come as a surprise, since the shorter pulse has about the same length as the dissipative lifetime of the target state, which is then more stable upon excitation. The pulse exhibits a double-bump structure, which is typical when dealing with strongly dissipative media [33,34]. As was the case for the 1 ps pulse the maximal pulse amplitude is shifted to the end of the pulse to minimize the effects of dissipation. On the other hand, only a single frequency dominates the Husimi transform of the GLOCT pulse, with a very minor component at about $\frac{1}{4}\omega_{02}$. This could suggest that only this frequency is necessary to improve the transfer yield and that the $\frac{1}{3}\omega_{02}$ component present in the 1 ps pulse is an artifact of the algorithm. Here again the simplicity of the pulse should render it experimentally realizable.

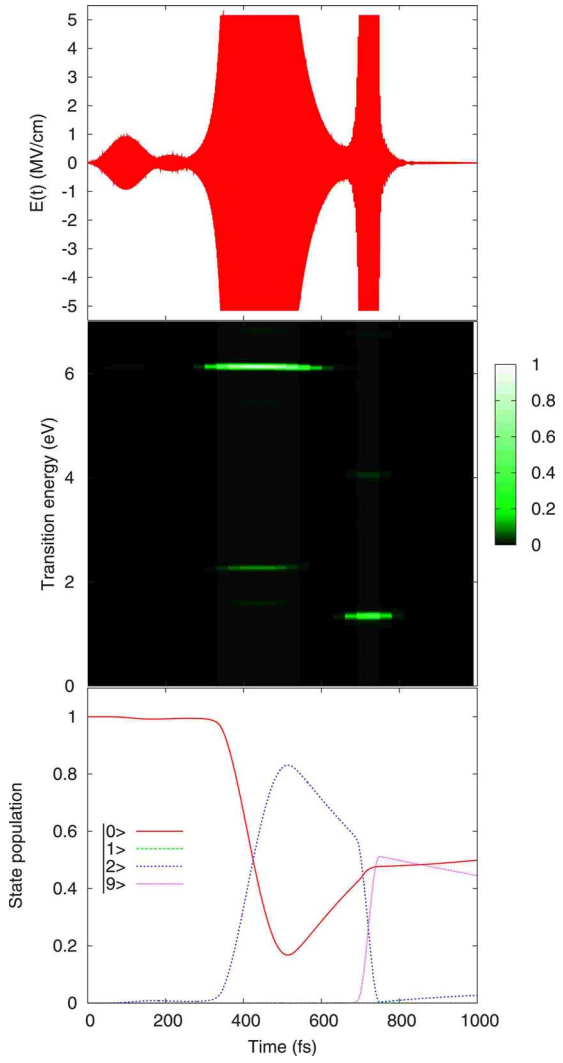

FIG. 4. (Color online) Population evolution (bottom panel), electric field (top panel), and its Husimi transform (central panel) for the excitation of state $|9\rangle$ using a 1 ps laser pulse. Local control parameters: $\alpha_0=0.1E_h/(a_0)^2$ and $E_{\max}=0.001E_h/ea_0$ (5.14 MV/cm).

C. Population of a semi-charge-transfer state

The selective population of the semi-charge-transfer state $|9\rangle$ represents a more challenging task, as it is not directly accessible from the ground state. State $|2\rangle$ represents a very natural intermediate in a two-step reaction pathway, but both states involved have a very short lifetime. The guide operator $\hat{G}$ was chosen as a stepwise excitation of state $|2\rangle$ ($t_2=500$ fs and $\sigma_2=100$ fs) and state $|9\rangle$ ($t_9=1000$ fs and $\sigma_9=200$ fs), with the density originally in the ground state ($t_0=0$ fs and $\sigma_0=200$ fs): $\hat{G}=O_{00}(t)|0\rangle\langle 0|+O_{22}(t)|2\rangle\langle 2|+O_{99}(t)|9\rangle\langle 9|$. The reference field was chosen as two nonoverlapping π pulses for $|0\rangle\rightarrow|2\rangle$ and $|2\rangle\rightarrow|9\rangle$ with a duration of 500 fs each, and fluences of 6.4 and 0.57 mJ/cm^2, respectively.

It can be seen from Fig. 4 that only 44.5% of the population can be transferred to the desired target state using a pulse of duration 1 ps and of fluence $F=17.1$ mJ/cm^2. The remaining part of the population is found mainly in the ground state. In this respect the GLOCT pulse can be considered state selective, albeit not very efficient. The pulse structure itself is interesting. The first step consists of the excitation of state $|2\rangle$ and the pulse exhibits a double-bump structure, as discussed previously, most probably to compensate the effects of strong dissipation. Furthermore, the same frequency distribution is revealed by the Husimi plot as for the simple excitation, namely, a dominant band at ω_{02} and two sidebands at $\frac{1}{3}\omega_{02}$ and $\frac{1}{4}\omega_{02}$. A second, slightly overlapping pulse with frequency tuned at the $|2\rangle\rightarrow|9\rangle$ transition appears at later time when the guide operator starts requiring population of the final target state. Even upon qualitative inspection of the resulting pulse, there is not much left to see from the reference field, the two nonoverlapping π pulses which give a target yield of 29.5%. This confirms that the GLOCT design equation is indeed responsible for the improved pulse efficiency.

As was the case for the excitation of the charge transfer state, we decided to reduce the duration of the control pulse to 500 fs in order to fight the negative effects of dissipation. Here again we chose the guide operator as a stepwise excitation from the ground state ($t_0=0$ fs and $\sigma_0=100$ fs) to state $|2\rangle$ ($t_2=250$ fs and $\sigma_2=100$ fs) and finally to state $|9\rangle$ ($t_9=500$ fs and $\sigma_9=100$ fs). The reference field has a double nonoverlapping π-pulse structure with fluences of 12.8 and 1.1 mJ/cm^2, respectively.

The reference field alone manages to transfer 46.4% of the population to the target state (see Fig. 5). This is already slightly better than the locally optimized 1 ps pulse, which has to cope with stronger dissipation on its longer time scale. Interestingly, the GLOCT algorithm manages to improve the transfer yield to 73.8% while maintaining the low field fluence ($F=15.6$ mJ/cm^2). The structure of the resulting field is very similar to that of the longer pulse at the early stage of the propagation, exhibiting the same type of double-bump structure as discussed above. As was the case for the excitation of state $|2\rangle$, less intense secondary frequency bands can be seen from the Husimi plot. The band at $\frac{1}{3}\omega_{02}$ almost completely disappears again. The main difference when comparing the longer and shorter GLOCT pulses comes at the later stage, for the second step of the excitation. The field component centered at the transition $|2\rangle\rightarrow|9\rangle$ is significantly overlapped with the end of the first bump exciting state $|2\rangle$. This seems to provide a more efficient transition to the desired final state and help fight the malicious effects of dissipation. As for the longer pulse, the second part of the excitation presents a band slightly above 4 eV, which is about three times the $|2\rangle\rightarrow|9\rangle$ transition frequency. As is often the case with optimal control theory, it is not clear why, but this frequency seems to be an important component of the locally optimal field.

D. Constant target operators

In order to assess the necessity of using time-dependent guide operators to achieve specific targets, we tested the locally optimal control algorithm with *constant* target operators. We chose to excite both states $|2\rangle$ and $|9\rangle$ with 1 ps

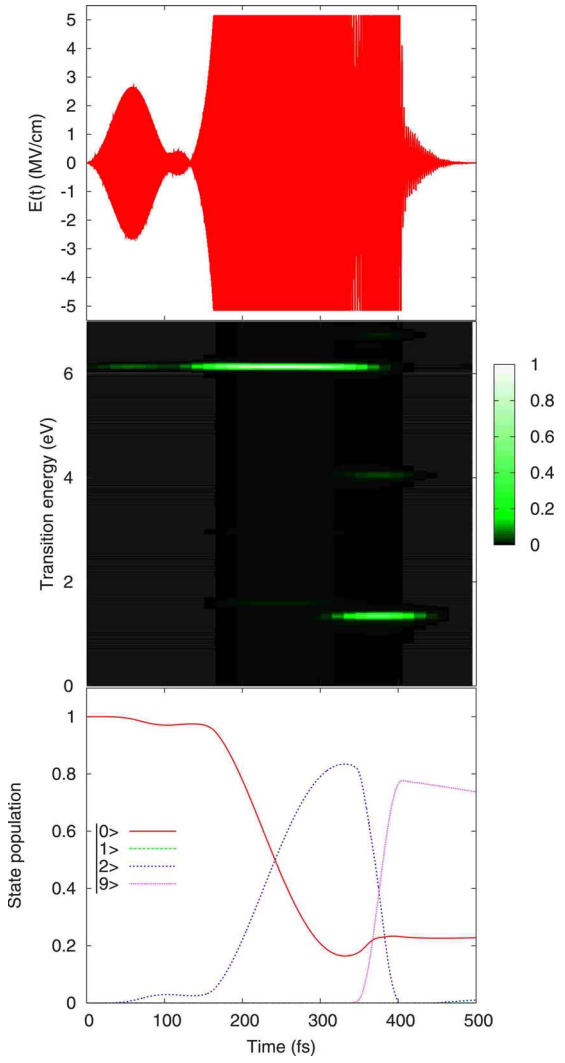

FIG. 5. (Color online) Population evolution (bottom panel), electric field (top panel), and its Husimi transform (central panel) for the excitation of state $|9\rangle$ using a 500 fs laser pulse. Local control parameters: $\alpha_0=0.1E_h/(a_0)^2$ and $E_{\max}=0.001E_h/ea_0$ (5.14 MV/cm).

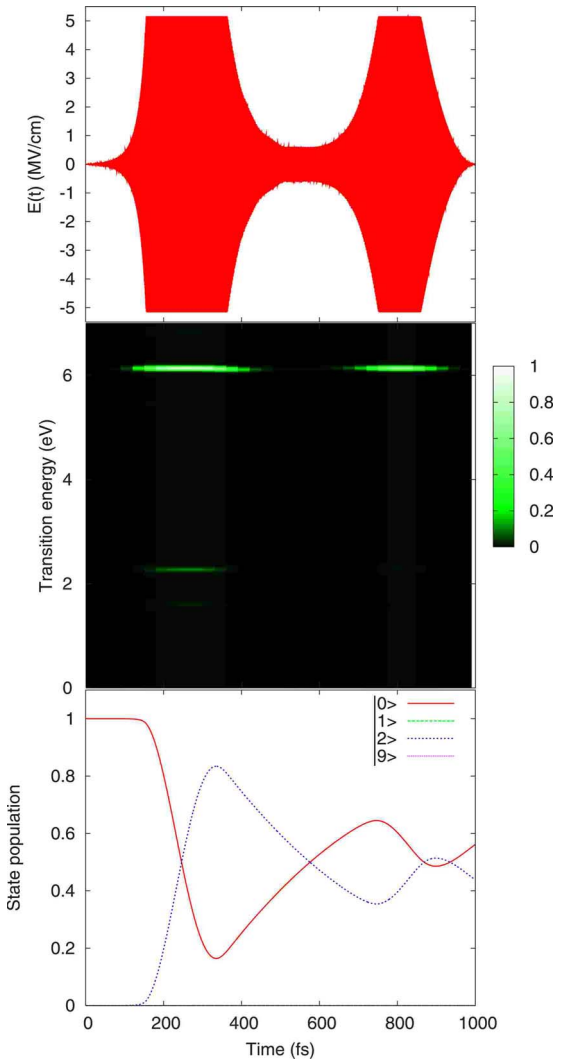

FIG. 6. (Color online) Population evolution (bottom panel), electric field (top panel), and its Husimi transform (central panel) for the excitation of state $|2\rangle$ using a 1 ps laser pulse. Local control parameters: constant target, $\alpha_0=0.1E_h/(a_0)^2$ and $E_{\max}=0.001E_h/ea_0$ (5.14 MV/cm).

pulses using the same reference fields as described above and with $\alpha_0=0.1E_h/(ea_0)^2$ and $E_{\max}=0.001E_h/ea_0$ (5.14 MV/cm). The resulting field for exciting the charge transfer state $|2\rangle$, using the target $\hat{G}=|2\rangle\langle 2|$, is shown in Fig. 6.

The transfer yield of 43.8% to the target state is slightly better than the one obtained with the moving target operator, which gave 42.9%. It thus seems that, for such a simple and direct mechanism, a time-dependent target function is unnecessary. On the other hand, the optimal pulse presents a more complicated structure than its GLOCT counterpart. It is interesting to note that the field intensity increases rapidly, to transfer most of the population from the ground state to the desired final state within about 500 fs. The frequencies observed in the Husimi transform are the same as previously mentioned. After a short period of free decay to the ground state, the field amplitude grows again to reach a second maximum at the end of the pulse, effectively pumping back the population to the desired state. The population change is somewhat damped as compared to the first pump pulse and should saturate at about 50% in the limit where many such short pump pulses are used.

The behavior of the algorithm for populating state $|9\rangle$ using a time-independent target $\hat{G}=|9\rangle\langle 9|$ is much more interesting (see Fig. 7). Whereas the reference field achieves 29.5% transfer and the GLOCT pulse a convincing improvement with 44.5% population, the constant target local control pulse reduces the yield to 25.0%. The failure of the algorithm can be rationalized by looking at the top panel of Fig. 7. All components of the field are clustered at the beginning of the pulse followed by a long period of free decay. It seems that the algorithm tries to pump the population too rapidly in the target state with many overlapping single-frequency pulses, thereby creating some nonoptimal interferences in the pulse. The nominal transfer yield after 400 fs is reasonably high, although not as good as for the 500 fs GLOCT pulse with

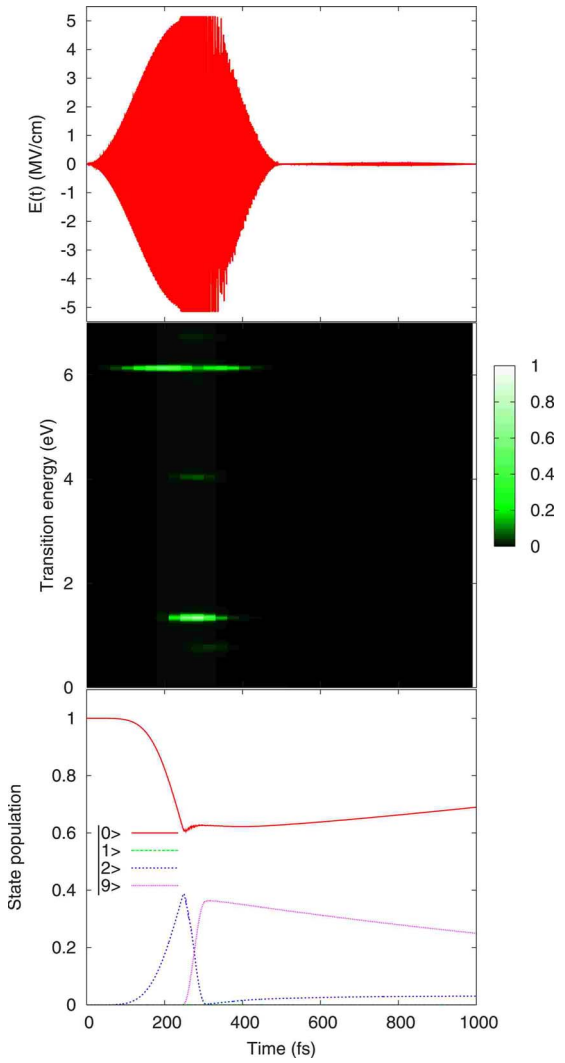

FIG. 7. (Color online) Population evolution (bottom panel), electric field (top panel), and its Husimi transform (central panel) for the excitation of state $|9\rangle$ using a 1 ps laser pulse. Local control parameters: constant target, $\alpha_0=0.1E_h/(a_0)^2$ and $E_{\max}=0.001E_h/ea_0$ (5.14 MV/cm).

time-dependent guide operator. In any case, the algorithm seems to have problems creating realistic fields using a time-independent target when the reaction path involves more than one step, as in the present case. Still, time-independent targets can be useful for *preserving* population over longer time periods rather than only achieving a given population at a prespecified control time. The limitations of the time-independent target are certainly due to the local nature of the algorithm, as global optimal control was shown to provide realistic pulses for similar stepwise excitation mechanisms.

V. CONCLUSION

We have presented ideas for controlling photoinduced processes in a dissipative environment. The guided locally optimal control algorithm is derived from the time-local pump-dump control scheme and extended to the density matrix formalism. We obtained an analytical expression for the optimal control pulse as a correction to a reference field. The solution of the equation does not require any backward propagation, as would be the case for the global optimal control theory. The control algorithm is numerically stable, even for multilevel systems.

In order to encourage the density to follow a desired reaction path, we advocate the use of time-dependent targets. We also directly constrained the field amplitude to maintain the low pulse fluence. The selective photoexcitation of charge transfer and semi-charge-transfer states of the LiCN molecule in a strong dissipative environment showed very encouraging results. On time scales comparable to the dissipative lifetime of the final target states, it was possible to design experimentally realizable pulses to achieve both desired targets and improve significantly the transfer yields, as compared to the reference fields. On time scales longer than the target state lifetime, the algorithm also performed well and helped refine the reference pulses to achieve the final target states more efficiently. It appeared that time-dependent guide operators were not necessary to achieve the desired target states when a direct reaction path is available, although they make the control fields simpler, and thus more experiment friendly. On the other hand, the benefits of moving targets were very important when dealing with final targets accessible only via more complicated pathways.

In closing, we note that the GLOCT algorithm could be improved iteratively, by using the electric field $E(t)$ as the reference field for the next propagation, i.e., $E_{\mathrm{ref}}^{(1)}(t)\rightarrow E^{(1)}(t)=E_{\mathrm{ref}}^{(2)}(t)\rightarrow E^{(2)}(t)=E_{\mathrm{ref}}^{(3)}(t)\rightarrow E^{(3)}(t)\cdots$, until convergence is achieved and the moving target approached as closely as possible. Again, no backward propagation is required.

ACKNOWLEDGMENTS

We gratefully acknowledge Dr. Tillmann Klamroth for fruitful discussions and for providing the CIS(D) data as well as his Husimi transform application. This work was supported by the Fonds Québécois de la Recherche sur la Nature et les Technologies (FQRNT) and the Sonderforschungbereich 450 of the Deutsche Forschungsgemeinschaft, "Analysis and Control of Ultrafast Photoinduced Processes" (Subproject No. C7).

[1] R. J. Levis, G. M. Menkir, and H. Rabitz, Science **292**, 709 (2001).
[2] M. Shapiro and P. Brumer, *Principles of the Quantum Control of Molecular Processes* (Wiley, Hoboken, NJ, 2003).
[3] G. Kurizki, M. Shapiro, and P. Brumer, Phys. Rev. B **39**, 3435 (1989).
[4] P. Brumer and M. Shapiro, Annu. Rev. Phys. Chem. **43**, 257 (1992).
[5] M. Shapiro and P. Brumer, J. Chem. Phys. **98**, 201 (1993).
[6] V. S. Batista and P. Brumer, Phys. Rev. Lett. **89**, 143201 (2002).
[7] A. P. Peirce, M. A. Dahleh, and H. Rabitz, Phys. Rev. A **37**, 4950 (1988).
[8] R. Kosloff, S. A. Rice, P. Gaspard, S. Tersigni, and D. J. Tannor, Chem. Phys. **139**, 201 (1989).
[9] S. Shi and H. Rabitz, J. Chem. Phys. **92**, 364 (1990).
[10] J. Somloi, V. A. Kazakov, and D. J. Tannor, Chem. Phys. **172**, 85 (1993).
[11] W. Zhu, J. Botina, and H. Rabitz, J. Chem. Phys. **108**, 1953 (1998).
[12] Y. Ohtsuki, W. Zu, and H. Rabitz, J. Chem. Phys. **110**, 9825 (1999).
[13] Y. Ohtsuki, K. Nakagami, W. Zhu, and H. Rabitz, Chem. Phys. **287**, 197 (2003).
[14] R. Xu, Y. Yan, Y. Ohtsuki, Y. Fujimara, and H. Rabity, J. Chem. Phys. **120**, 6600 (2004).
[15] J. D. Farnum and D. A. Mazziotti, Chem. Phys. Lett. **416**, 142 (2005).
[16] T. Cheng and A. Brown, J. Chem. Phys. **124**, 144109 (2006).
[17] C. Gollub, M. Kowalewski, and R. de Vivie-Riedle, Phys. Rev. Lett. **101**, 073002 (2008).
[18] K. Blum, *Density Matrix Theory and Applications* (Plenum Press, New York, 1996).
[19] N. Gisin and I. C. Percival, J. Phys. A **25**, 5677 (1992).
[20] K. Molmer, Y. Castin, and J. Dalibar, J. Opt. Soc. Am. B **10**, 524 (1993).
[21] M. B. Plenio and P. L. Knight, Rev. Mod. Phys. **70**, 101 (1998).
[22] R. Kosloff, A. D. Hammerich, and D. J. Tannor, Phys. Rev. Lett. **69**, 2172 (1992).
[23] M. Sugawara and Y. Fujimara, J. Chem. Phys. **100**, 5646 (1994).
[24] D. J. Tannor, *Molecules in Laser Fields* (Dekker, New York, 1992).
[25] Y. Ohtsuki, H. Kono, and Y. Fujimura, J. Chem. Phys. **109**, 9318 (1998).
[26] Y. Ohtsuki, Y. Yahata, H. Kono, and Y. Fujimura, Chem. Phys. Lett. **287**, 627 (1998).
[27] Y. Zhao and O. Kühn, J. Phys. Chem. A **104**, 4882 (2000).
[28] F. L. Yip, D. A. Mazziotti, and H. Rabitz, J. Phys. Chem. A **107**, 7264 (2003).
[29] S. Beyvers and P. Saalfrank, J. Chem. Phys. **128**, 074104 (2008).
[30] A. Kaiser and V. May, J. Chem. Phys. **121**, 2528 (2004).
[31] I. Serban, J. Werschnik, and E. K. U. Gross, Phys. Rev. A **71**, 053810 (2005).
[32] K. Husimi, Proc. Phys. Math. Soc. Jpn. **22**, 264 (1940).
[33] S. Beyvers, Y. Ohtsuki, and P. Saalfrank, J. Chem. Phys. **124**, 234706 (2006).
[34] J. C. Tremblay, S. Beyvers, and P. Saalfrank, J. Chem. Phys. **128**, 194709 (2008).
[35] T. Klamroth, Phys. Rev. B **68**, 245421 (2003).
[36] J. C. Tremblay, T. Klamroth, and P. Saalfrank, J. Chem. Phys. **129**, 084302 (2008).
[37] P. Krause, T. Klamroth, and P. Saalfrank, J. Chem. Phys. **123**, 074105 (2005).
[38] W. H. Press, S. A. S. A. Teukolsky, W. T. Vetterling, and B. P. Flannery, *Numerical Recipes in FORTRAN 77: The Art of Scientific Programming* (Cambridge University Press, Cambridge, U.K., 1986).
[39] J. C. Tremblay and T. Carrington, Jr., J. Chem. Phys. **121**, 11535 (2004).
[40] V. Gorini, A. Kossakowski, and E. C. G. Sudarshan, J. Math. Phys. **17**, 821 (1976).
[41] V. Gorini and A. Kossakowski, J. Math. Phys. **17**, 1298 (1976).
[42] G. Lindblad, Commun. Math. Phys. **48**, 119 (1976).
[43] R. Kosloff, M. Ratner, and W. B. Davis, J. Chem. Phys. **106**, 7036 (1997).
[44] T. Klamroth, J. Chem. Phys. **124**, 144310 (2006).